ロシア・東部バイカル地域におけるマントル進化

Mantle evolution beneath the Eastern Baikal Region, Russia

Konstantin LITASOV*,**・Yury LITASOV**,***・Hirokazu FUJIMAKI****
Tsuyoshi MIYAMOTO*・Hiromitsu TANIGUCHI*

Key words : upper mantle, xenolith, peridotite, pyroxenite

Abstract

The genesis of major groups of xenoliths from the Late Cenozoic volcanic rocks of the eastern part of Baikal Rift System is considered on the basis of petrology and mineral chemistry. Reconstructed mantle sections beneath the Vitim field appear to be more complex than beneath the Udokan field due to significant modification by hydrous metasomatic melts. Peridotite xenoliths from the Miocene picrobasalts represent garnet and spinel depth facies. Pyroxenite xenoliths are interpreted as products of three types of the melt. The first forms Cr-diopside pyroxenites, it is an interstitial melt migrating through peridotite, and it is similar to melts described in peridotite massifs as undergoing percolative fractionation. Textural and compositional relationships indicate melt segregation and fractionation under the high-pressure conditions towards Al-rich pyroxenites and - at shallower levels - towards sp-websterites. The second and third melt types form the hydrous veins and megacrystic pyroxenites, respectively. Both were crystallized in larger channels relative to the first melt type, whereby the amphibole- and phlogopite-bearing assemblages may represent smaller channels on a scale of dozen centimeters.

Three series of peridotite xenoliths from Pliocene basanites were determined: (1) high-T garnet and spinel lherzolites, (2) low-T spinel lherzolites and harzburgites, (3) low-T titaniferous spinel lherzolites. Protogranular peridotites of the Series 1 represent primitive to moderately depleted mantle from the depths 60-80 km at T=1100-1250℃. Trace element patterns in clinopyroxenes are indicative of low degree partial melting of the primitive mantle. Peridotites of the Series 2 correspond to the depths 40-50 km at T=800-900℃. Titaniferous peridotites enriched in pyroxenes and spinel were newly detected. They have a mosaic equigranular texture and are suggested to be a rare type of melt/mantle interaction. T-estimations within 750-850℃ projected to a geotherm allow to interprete their correspondence to the uppermost mantle section (40-50 km depth). High Ti content (TiO_2=0.55% in the bulk rock) may characterize a

* Center for Northeast Asian Studies, Tohoku University
** United Institute of Geology, Geophysics and Mineralogy, Novosibirsk, Russia
*** Research Institute of Materials and Resources, Akita University
**** Graduate School of Science, Tohoku University

metasomatizing melt generated from ilmenite- and/or phlogopite-bearing source. Clinopyroxene REE patterns $(La/Yb)_n$=0.01-0.08) reveal an evidence for MORB-like composition of coexisting melt.

Xenoliths from the Pliocene basanites of Kuas Lake (Udokan field) show variation of unhydrous depletion and enrichment of lower lithosphere. Xenoliths correspond to spinel facies and may be divided into lherzolite, harzburgite and dunite, and websterite groups. Depleted nodules contain clinopyroxene enriched in LREE and depleted in HFSE. This enrichment is explained by reactive percolation of small melt fraction and accompanying melting of peridotites. Harzburgite-dunite veins seem to be located at the lower part of mantle column and have been formed by olivine-producing reaction with increasing of melt fraction. Lherzolite and websterite are located at the middle and upper part of column and have been formed by pyroxene-producing reaction with decreasing of melt fraction.

1. Introduction

Mantle xenoliths are often found in many alkaline basalt localities over the Baikal rift system. In the eastern part of it, two volcanic fields may be defined: Vitim and Udokan (Fig.1a). Abundant mantle and lower crustal xenoliths were found in the Late Miocene - Pleistocene volcanics, which are presented by

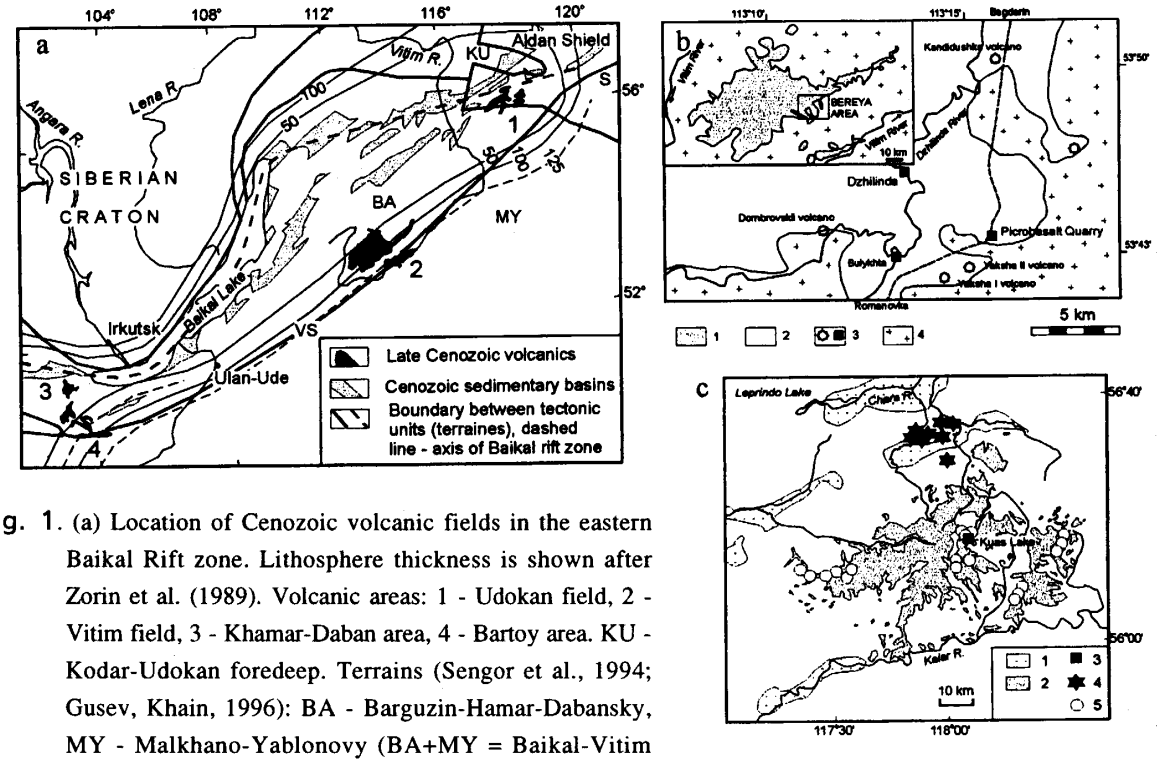

Fig. 1. (a) Location of Cenozoic volcanic fields in the eastern Baikal Rift zone. Lithosphere thickness is shown after Zorin et al. (1989). Volcanic areas: 1 - Udokan field, 2 - Vitim field, 3 - Khamar-Daban area, 4 - Bartoy area. KU - Kodar-Udokan foredeep. Terrains (Sengor et al., 1994; Gusev, Khain, 1996): BA - Barguzin-Hamar-Dabansky, MY - Malkhano-Yablonovy (BA+MY = Baikal-Vitim complex terrain). VS - Vitim suture, S - Stanovoy suture. (b) Schematic map of the Vitim volcanic field and Bereya area: 1-2 - Cenozoic basalts, 3- volcanic cones and xenolith localities, 4- Paleozoic granites and metamorphic rocks. (c) Schematic map of the Udocan volcanic field after Rasskazov et al. (1997): 1- Cenozoic sedimentary basins, 2- Late Cenozoic volcanics, 3- xenolith locality, 4 - melaleucitite/melanephelinite, and 5 - trahyte volcanoes.

nephelinites and basanites in the Udokan field and picrobasalts and basanites in the Vitim.

The Vitim volcanic field is a reference object in the Baikal rift system (BRS). Many authors reported data for Vitim xenoliths, however their diversity is wide enough to proclaim just the beginning stage of Vitim mantle study. Some detail works were devoted to garnet peridotites (Ionov et al., 1993; Glaser et al., 1999), pyroxenites and hydrous veined assemblages from Vitim picrobasalts (Ashchepkov et al., 1994; Litasov, 1996). Rasskazov (1986) and Litasov et al. (1999) reported preliminary results for the Udokan xenoliths.

The main goal of this review is to discuss current hypotheses of xenolith origin and to summarize data for xenoliths from the volcanic fields of the eastern part of the BRS. Models of mantle evolution and mantle/melt interaction are considered, as well.

2. Geological background and host volcanics

Volcanism of the Vitim and Udokan fields was caused by a plume activity on the periphery of the BRS. The Vitim field is located above the lithospheric slope (the lithospere thickness increases from NW to SE from 50 to 125 km (Fig. 1). It was attracted by the Early Paleozoic suture zone between the Mongolian microcontinent and Siberian platform. Also, this suture zone is a southern boundary of the Khamar-Daban-Barguzin microcontinent (terrain) (Fig. 1) (Sengor et al., 1994).

Within the Vitim field, several volcanic areas were detected. The most of xenolith-bearing volcanics occur within the Bereya area (Fig.1b), which is the best studied in terms of chemical composition and age determinations for the volcanics. K-Ar dating indicates at least three eruption stages in the Bereya area (Rasskazov et al., 1996): (1) Middle Miocene stage (16-14 Ma) manifested by eruptions of picrobasalt and basaltic andesite with subordinate high-Ti olivine tholeiite, (2) Late Miocene stage (～8 Ma) is characterized by eruptions of basanite to alkaline olivine basalt and olivine tholeiite, (3) Plio-Pleistocene stage (2-0.8 Ma) is represented by basanite to phonobasanite.

The xenolith-bearing picrobasalts are complicated for the age determination due to an alteration and abundant xenogenic material. Recent K-Ar estimation of the aphanitic groundmass indicates the age of 16.3±1.1 Ma (Esin et al., 1995). Selected major element and isotopic data for the picrobasalt and xenolith-bearing basanite are presented in Table 1.

The Udokan field is located at a junction of the BRS rift structure with young, relatively fertile lower lithospheric domain and Aldan shield of the Siberian Craton with the ancient Archean depleted mantle. Composition of the host alkaline basalts of the Udokan field reflects ancient mantle heterogeneity and different tectonic and plume regimes (Rasskazov et al., 1997). Spatial variations of basalt compositions are stimulated by the Cenozoic reactivation of the Kodar-Udokan fold zone accompanied by sedimentation in Chara depression near 14 Ma ago. Contemporaneously, the first eruption of melanephelinite-melaleucitite

Table 1. Composition of host basalts and bulk peridotite xenoliths.

	1	2	3	4	5	6	7	8	9	10	11	12
Sample	C-215	Dzh	77-6	313-1	313-113	314-6	D-871	D-73	D-43	74-8	74-5	74-117
SiO_2	41.81	46.09	44.77	44.15	43.60	44.45	44.28	43.85	45.67	44.09	43.93	45.89
TiO_2	2.11	2.65	2.65	0.17	0.10	0.06	0.07	0.12	0.55	0.04	0.13	0.22
Al_2O_3	9.45	14.05	14.60	4.37	2.54	1.53	2.71	1.75	5.22	1.35	2.70	5.15
Cr_2O_3				0.37	0.34	0.53	0.44	0.31	0.88	0.60	0.43	0.28
Fe_2O_3			3.11				2.42	3.02	2.52	1.15	1.62	2.24
FeO	12.06*	12.24*	9.17	7.92*	8.65*	7.53*	5.93	5.39	4.31	6.92	7.26	5.47
MnO	0.17	0.14	0.16				0.12	0.14	0.10	0.14	0.14	0.14
NiO							0.23	0.18	0.25	0.27	0.26	0.19
MgO	15.53	8.77	8.81	38.50	43.30	43.75	38.54	43.60	36.50	44.54	40.43	34.75
CaO	9.62	8.03	8.69	3.00	1.43	1.40	3.70	1.30	2.90	1.17	2.82	4.97
Na_2O	0.77	4.31	3.29	0.25	0.27	0.28	0.50	0.13	0.32	0.23	0.41	0.62
K_2O	1.46	2.60	1.17	0.37	0.15	0.11	0.05	0.06	0.04	0.08	0.12	0.09
P_2O_5	0.67	0.66	0.70									
LOI	6.00		2.44									
Total	99.65	99.54	99.56	99.10	100.38	99.64	98.99	99.85	99.26	100.58	100.25	100.01
Mg#	69.6	56.1	56.7	89.7	89.9	91.2	89.4	90.6	90.8	90.9	89.3	89.2

1- Miocene picrobasalt (15 Ma), Vitim field; 2- Pliocene basanite (1.8 Ma), Vitim field; 3- Pliocene basanite (3 Ma), Udokan field. 4-6- peridotites from Miocene picrobasalts, Vitim field (Ionov et al., 1993): 4- ga lherzolite, 5- ga-sp lherzolite, 6- sp lherzolite; 7-9- peridotites from Pliocene basanites, Vitim field: 7- high-T sp lherzolite, 8- low-T sp lherzolite, 9- low-T Ti-rich lherzolite; 10-12- peridotites from Pliocene basanites, Udokan field: 10- sp harzburgite, 11- sp lherzolite, 12- composite lherzolite/websterite xenolith (lherzolite zone). *- total Fe as FeO.

lavas and formation of numerous volcanic cones and subvolcanic bodies took place (Fig.1c). At the next stage, the volcanic activity was shifted towards the south and manifested as volumunous eruptions of alkali olivine basalts and trahytes. K-Ar-dating of volcanics indicated several eruption episodes in accordance with the volcanism migration in the east-west direction: 9.6-8.2; 4.0-2.6; 1.7-0.002 Ma (Rasskazov et al., 1998).

Xenolith-bearing basanites were found in basaltic outcrops near Kuas Lake. The group of Kuas trachyte volcanoes is dated at 3.5-2.6 Ma. The trachytes of studied outcrop have ages 3.3 Ma in the upper part and 3 Ma in the lower part. Thus, we suggest the same age for the xenolith-bearing lavas which are located in the middle part of stratigraphic sequence. The basanite compositions are presented in Table 1.

3. Review of analytical methods

Original data used in this work have been obtained by the following techniques: Major elements for the xenoliths' bulk were measured by XRF and "wet chemistry" in the United Institute of Geology, Geophysics and Mineralogy (UIGGM), Novosibirsk, the Institute of Geochemistry SB RAS, Irkutsk, the Institute of the Earth Crust, Irkutsk. Major elements in xenolith minerals were measured by EPMA (Camebax Micro) in UIGGM. Trace elements in xenolith minerals were measured by SIMS in the Institute of Microelectronics, Yaroslavl', Russia.

Table 2. Systematics of deep-seated xenoliths and megacrysts of the Vitim and Udokan volcanic field.

Vitim field, Miocene picrobasalts	
Type I	**Type II**
Primitive ga and sp lherzolites	Al-rich ga clinopyroxenites
Metasomatically modified xenoliths: a) phl-bearing lherzolites b) amp-bearing lherzolites c) ilm orthopyroxenites and harzburgites Vein types in peridotites (composite type I/type II nodules): a) amp-phl veins b) amp-phl-cpx-opx veins c) phl-cpx veins	Megacryst assemblages: a) Cr-rich websterites b) ga websterites and cpx megacrysts c) cpx-megacrysts, including ilm-phl-bearing nodules d) ilmenite megacrysts
Cr-diopside pyroxenites: a) ga and sp websterites b) Al-poor websterites	Lower crystal/uppermost mantle cumulates: a) ga granulites b) ga clinopyroxenites and gabbroes c) sp websterites
Vitim field, Pliocene basanites	
Peridotites: Gr.1 High-T ga and sp lherzolites Gr 2 Low-T sp peridotites a) harzburgites b, c) lhezrolites (c – tabular texture) Gr 3 Low-T Ti-rich sp lherzolites	Megacryst assemblage: a) ga clinopyroxenites and cpx megacrysts b) garnet c) ilmenite d) Ti-biotite e) alkali feldspars
Cr-diopside pyroxenites a) High-T ga and sp websterites b) Low-T sp websterites c) Al-poor websterites	Lower crustal/uppermost mantle cumulates: a) sp websterites Type IIa 5. Scarn-like clinopyroxenites
Udokan field, Pliocene basanites	
Sp peridotites: a) harzburgites and dunites 6) lherzolites	Ga orthopyroxenites Megacryst assemblages: a) clinopyroxene b) alkali feldspar c) Ti-biotite
Cr-diopside sp pyroxenites	Lower crustal xenoliths

4. Systematics of xenoliths, petrography and major element chemistry

Several major groupings of peridotites, pyroxenites and megacrysts were distinguished among the xenoliths from the Miocene picrobasalts and Pliocene basanites of the Vitim field and the Pliocene basanites of the Udokan field (Table 2) on the basis of mineral assemblages and major element composition of minerals. Major element compositions of the bulk rocks and selected xenolith minerals are given in Tables 1 and 3.

4.1. Xenoliths from the Miocene picrobasalts, Vitim field

4.1.1. Primitive garnet and spinel lherzolites

The major part of the Vitim xenoliths is represented by lherzolite (Fig.3). It includes both spinel (sp)

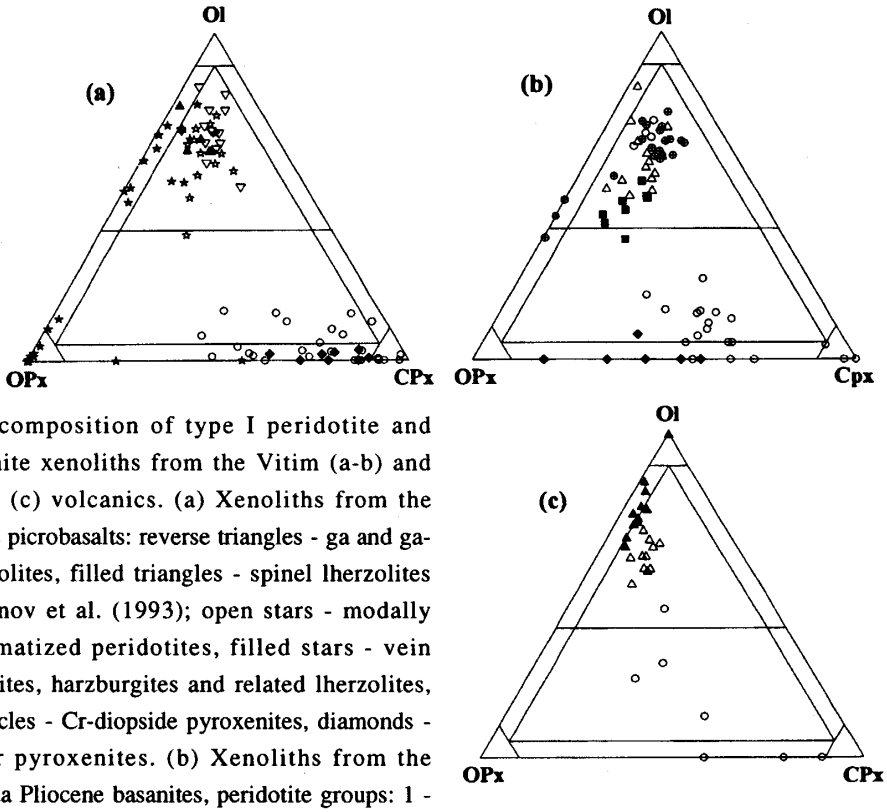

Fig. 2. Modal composition of type I peridotite and pyroxenite xenoliths from the Vitim (a-b) and Udokan (c) volcanics. (a) Xenoliths from the Miocene picrobasalts: reverse triangles - ga and ga-sp-lherzolites, filled triangles - spinel lherzolites after Ionov et al. (1993); open stars - modally metasomatized peridotites, filled stars - vein pyroxenites, harzburgites and related lherzolites, open circles - Cr-diopside pyroxenites, diamonds - Al-poor pyroxenites. (b) Xenoliths from the Dzhilinda Pliocene basanites, peridotite groups: 1 - crossed circles, 2 - triangles, 3 - squares; pyroxenite sympols are similar to (a). (c) Xenoliths from the Kuas Lake Pliocene basanites: filled triangles - harzburgites and dunites, open triangles - lherzolites, circles - websterites and pyroxene-rich lherzolites.

and garnet (ga) varieties and completely covers a transition between them. Textural features are almost the same for both facies. The most samples have medium- to coarse-grained protogranular textures (Mercier and Nicolas, 1975) (Fig.3b-c). Tabular equigranular sp-lherzolite is also found occasionally. The tabulation is controlled by a preferable orientation of elongated 3-6 mm olivine (ol) grains (Fig.4a).

Olivine from the lherzolites is compositionally uniform and ranges from Fo89 to Fo91. NiO contents overlap those of the mantle array (Takahashi, 1986). The variations in primary orthopyroxene (opx) and clinopyroxene (cpx) compositions are wide. Mg-number varies within 89-91% in the opx from most ga- and sp-ga-lherzolites, 88-91% in the cpx from ga-lherzolites, and 87-93% in the cpx from sp-lherzolites. Cr#=100Cr/(Cr+Al) of primary sp ranges from 3 to 40%. Mg-number is more uniform ranging 74-84% for sp-ga-lherzolites, and 70-83% for sp-peridotites. Mg-number in ga ranges from 83 to 85% for ga-peridotites and from 82 to 86% for sp-ga-peridotites.

4.1.2. Metasomatically modified xenoliths

Xenolith assemblages containing hydrous minerals (Table 2) vary from the vein material crystallized from hydrous melts to peridotites containing just scarce hydrous minerals.

Metasomatic veins in peridotites are composed of amphibole (amp), phlogopite (phl) and pyroxenes in

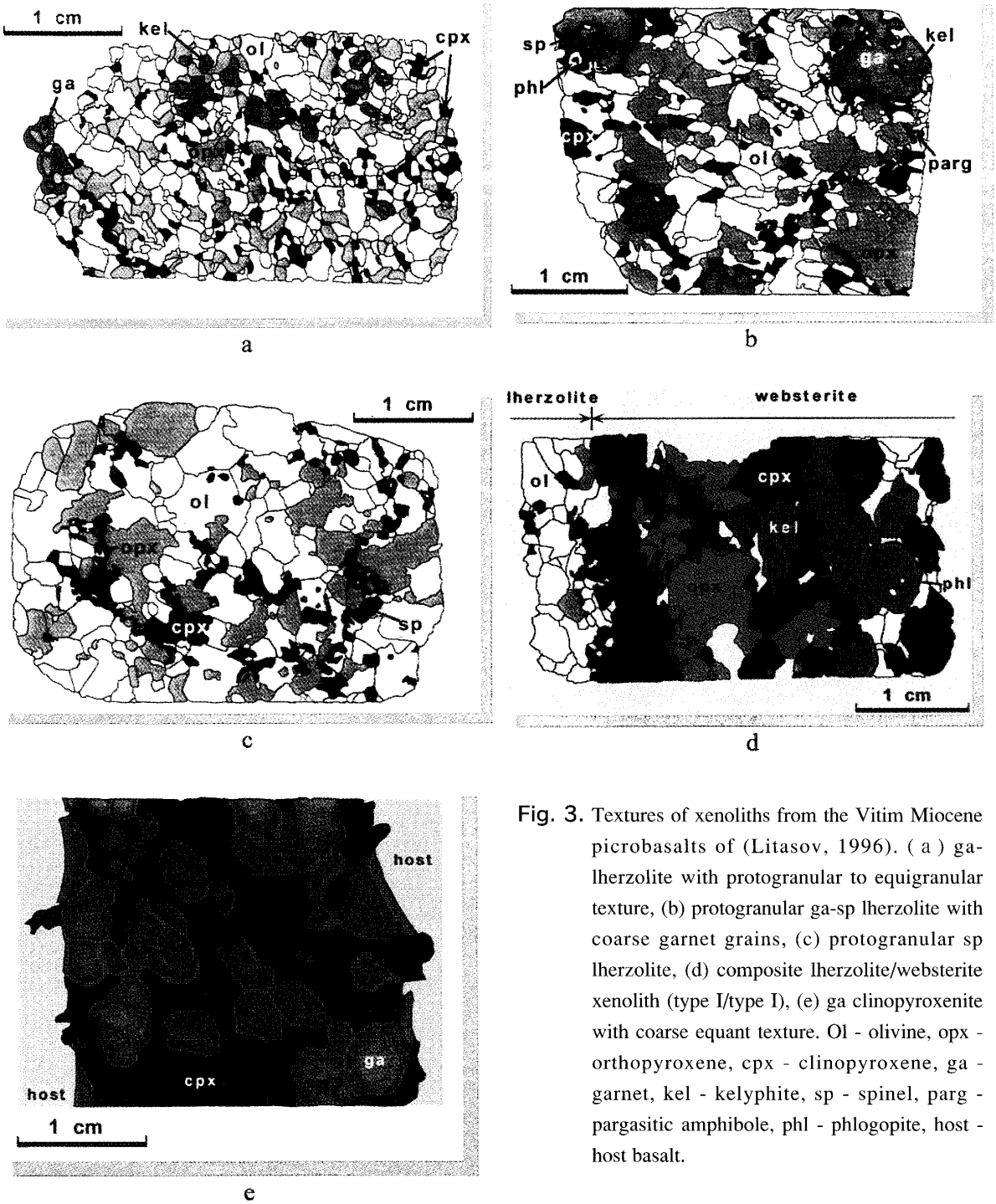

Fig. 3. Textures of xenoliths from the Vitim Miocene picrobasalts of (Litasov, 1996). (a) ga-lherzolite with protogranular to equigranular texture, (b) protogranular ga-sp lherzolite with coarse garnet grains, (c) protogranular sp lherzolite, (d) composite lherzolite/websterite xenolith (type I/type I), (e) ga clinopyroxenite with coarse equant texture. Ol - olivine, opx - orthopyroxene, cpx - clinopyroxene, ga - garnet, kel - kelyphite, sp - spinel, parg - pargasitic amphibole, phl - phlogopite, host - host basalt.

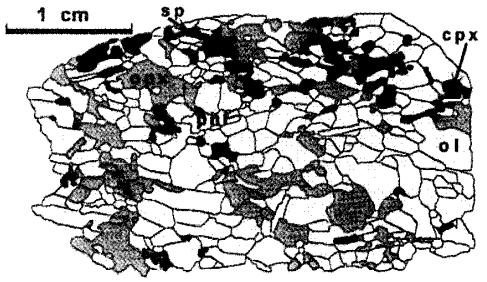

Sample No 314-669.
Spinel lherzolite containing interstitial phlogopite.

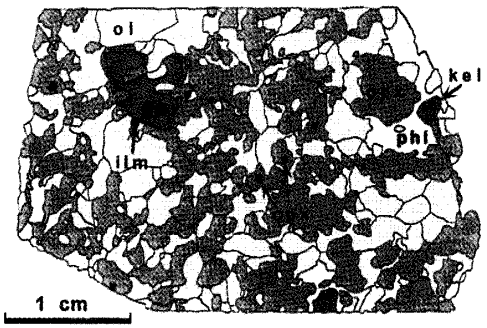

Sample No L-10-2. Garnet harzburgite containing interstitial phlogopite around garnet.

a

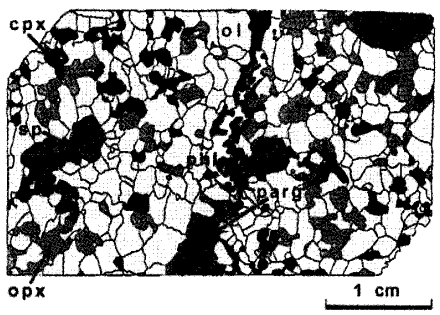

Sample No 313-699. Spinel-garnet lherzolite cut by phlogopite-clinopyroxene veinlet.

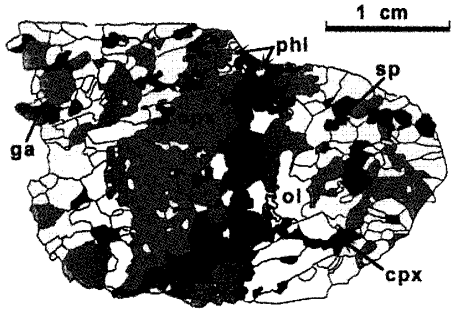

Sample No 313-700. Spinel-garnet lherzolite cut by phlogopite-pargasite vein. Orthopyroxene reaction band develops around the vein.

b

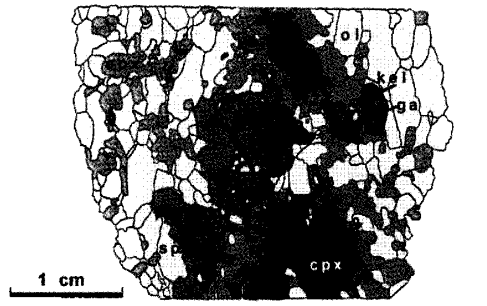

Sample No 626-100. Amphibole vein in spinel-garnet lherzolite.

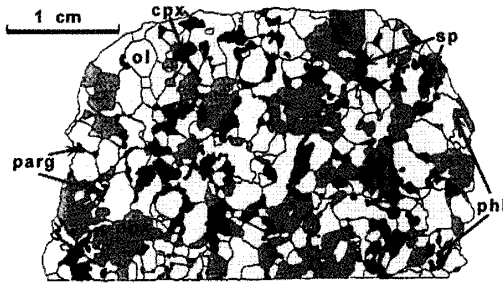

Sample No 313-707. Spinel lherzolite with a protogranular texture and interstitial pargasite coronas around spinel.

c

Fig. 4. Textures of metasomatically modified xenoliths from the Vitim Miocene picrobasalts (Litasov, 1996). (a) phl-bearing sp-lherzolite with tabular equigranular texture and "reactionary" ga-harzburgite, (b) cpx-phl veinlet in ga-lherzolite and amph-phl vein in ga-sp lherzolite (c) amph vein in ga-sp-lherzolite and sp-lherzolite with dispersed amphibole. Ol - olivine, opx - orthopyroxene, cpx - clinopyroxene, ga - garnet, kel - kelyphite, sp - spinel, parg - amphibole, phl - phlogopite, ilm - ilmenite.

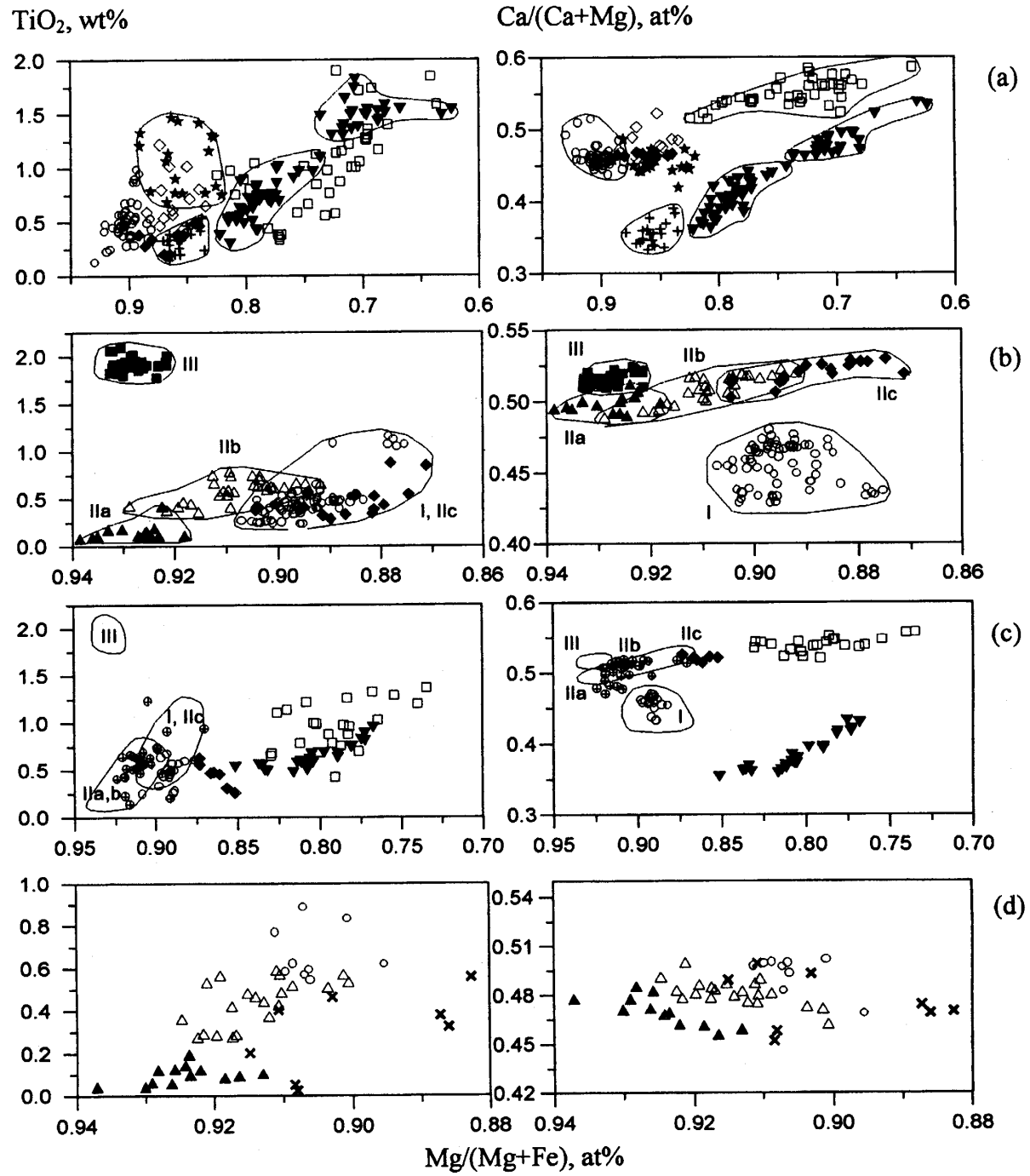

Fig. 5. Variation diagrams for clinopyroxene from the Vitim (a-c) and Udokan (d) xenoliths. (a) Pyroxenite from the Miocene picrobasalts: stars - hydrous veins, orthopyroxenites, and related amph-phl-bearing lherzolites, open circles - Cr-diopside pyroxenites, filled diamonds - Al-poor websterites, open diamonds - Al-rich ga-clinopyroxenites, crosses - Cr-rich websterites of megacryst trend, reverse triangles - cpx-megacrysts and related pyroxenites, squares - lower crustal granulites and Al-augite websterites. (b) Peridotites from the Pliocene basanites, open circles -ga- and sp-lherzolites, gr.1, filled triangles.- harzburgites and lherzolites, gr.2a, open triangles - lherzolites, gr.2b, diamonds - Al-poor pyroxene-rich lherzolites, gr.2c, squares - Ti-rich lherzolites, gr.3. (c) Pyroxenites from the Pliocene basanites: open circles - High-T ga- and sp-websterites, crossed circles - Low-T sp-websterites, other symbols as in (a), named fields - peridotite composition, after fig. b. (d) Xenoliths from the Kuas Pliocene basanites: filled triangles - harzburgites and dunites, open triangles - lherzolites, circles - websterites, Xs- cryptically metasomatized nodules.

variable ratios (Litasov, 1996), and can be divided into three major types: Amp-phl, amp-phl-opx-cpx, and phl-cpx. Monomineral amp-veinlets and interstitial amp and/or phl in ga- and sp-lherzolites have been found (Fig.4). Cpx has Mg-number of 84-89 and high TiO_2 (1.0-1.6 wt.%) relative to cpx from pyroxenites with a similar Mg-number (Fig.5a). Amp is represented by titaniferous pargasites-kaersutites containing TiO_2=2.5-6.1 wt.%, Cr_2O_3=0.8-1.7 wt.%, K_2O=1.5-2.2 wt.%, and F=0-0.15 wt.%.

Metasomatic orthopyroxenites are not typical among the xenoliths of alkaline basalts; their modal mineralogy is opx 81-96%, ga 0-12%, cpx 0-7%, ilm 0-3%, phl 0-4%, olv 0-2%, amp - trace. In some composite samples, the orthopyroxenites are found along the contacts between vein assemblages and lherzolite wall minerals. Orthopyroxenite mineral compositions are similar to those from hydrous amp-phl veins. Compositional zoning of peridotite minerals in contact with orthopyroxenite is much greater than at contacts with small hydrous veinlets. Ilmenite contains 0.5-2.8 wt.% Cr_2O_3 and 8.2-12.9 wt.% MgO.

4.1.3. Cr-diopside pyroxenites

This group is characterized by Cr-rich diopsidic cpx and, therefore, is similar to Group I xenoliths defined by Frey and Prinz (1978). Usually Cr-diopside pyroxenites (Table 2) are represented by websterites including ga-, ga+sp-, and sp-bearing varieties. The ga-pyroxenites mostly have coarse equant to protogranular textures and variable mineral modes (Fig.3e). Minor amounts of phl were found in some nodules. In sp-websterites, the modal amounts of sp reach up to 6%. Composite nodules of websterite and lherzolite with irregularly curved boundaries showing the websterites as veins in the lherzolite are widespread (Fig.3d).

The mineral chemistry of the Cr-diopside websterites resembles that of the lherzolites, although the Mg-number of all pyroxenite minerals is slightly lower. Cpx is characterized by high TiO_2 (0.2-1.0 wt.%) relative to lherzolitic. Opx (Mg#=88-90) and ga (Mg#=80-85) compositions are similar to lherzolitic minerals.

Al-poor subgroup websterites have coarse-equant textures and generally low modal abundance of aluminous phases. Mineral chemistry with low Al_2O_3 is diagnostic for this group: mineral compositions are close to those from depleted peridotite nodules worldwide differing only in the lower Mg-number (85-90). Cpx contains 3.1-4.1 wt.% Al_2O_3 and has constant Ca#=Ca/(Ca+Mg) of approximately 0.47 (Fig.5a). Interstitial graphite was found in one sample.

4.1.4. Al-rich pyroxenites

Al-rich ga-clinopyroxenites have coarse-equant to typical adcumulate textures, with modal contents of ga generally in the range of 20-50%, although exceptionally up to 56%. Cpx has high Mg-number (83-88)

similar to those of most magnesian megacrysts, however it has also high Al_2O_3 (6.2-10.5 wt.%) and low Cr_2O_3 (0.1-0.2 wt.%), and consistently high Ca# (Fig. 5a).

4.1.5. Megacryst assemblages

We consider the cpx-megacrysts to be related to Group II nodules of Frey and Prinz (1978) because they form a continuous trend in variation diagrams, and are characterized by decreasing Mg and Cr, and increasing Ti, Al, Na, and Ca abundances (Fig. 5a), in common with Al-augite-rich Ga-websterites and clinopyroxenites. Two subgroups were detected: (a) Cr-rich megacrystic websterites and clinopyroxenites, and (b) Cr-poor megacrystic ga-websterites, clinopyroxenites and cpx-megacrysts, Al-Ti-Na-rich cpx-megacrysts with ilmenite and phlogopite inclusions, and ilm-cpx-symplectites (graphic intergrowths).

The appearance and color of the a-subgroup megacrysts is similar to those pictured by Menzies et al. (1987a, Plate 1, Col.3). The compositions of the cpx plot to the high-Mg end of a trend defined by the subroup a and b megacrystic pyroxenites, with consistently lower Ca (Fig.5a).

The average modal composition of subgroup b ga-websterites is cpx 78%, ga 14%, opx 8%. Cpx form a continuous trend from compositions similar to those of a-subgroup cpx towards high TiO_2, Al_2O_3, Na_2O and CaO (Fig.5a), indicating a genetic link and arbitrary distinction between these two subgroups. Ilmenite from subgroup b megacrystic pyroxenites contains 5-6.5 wt.% MgO. Phlogopite has 7-8.4 wt.% TiO_2 and low Mg-number in the range 64-77.

4.1.6. Low presure cumulates

These samples consist of three subgroups: (a) opx-free ga-clinopyroxenites and gabbros with adcumulate and anhedral-granular textures; (b) ga-granulites and amphibolites with metacumulate to granoblastic texture; and (c) sp-websterites with metacumulate texture. These xenoliths have very variable modal composition and may contain cpx, opx, ga, sp, amp, phl/biotite, plagioclase, sanidine, scapolite, ilmenite, and titanomagnetite. Litasov (1999) treats their subdivisions and characteristics in detail. They are grouped together on the basis of high Ca# cpx (Fig. 5a) and similarity in P-T-conditions. Ga-clinopyroxenite and gabbro of group (a) contain cpx, which composition is close to the most Fe-rich subgroup (b) megacrysts (Mg-number 63-83). These varieties also contain up to 9.5 wt.% of Al_2O_3. Cpx from group (c) sp websterites contains up to 0.4 wt.% Cr_2O_3 and forms a compositional trend towards Cr-diopside pyroxenites.

4.2. Xenoliths from Pliocene basanites, Vitim field

4.2.1. Garnet and spinel lherzolites

Three series of peridotite xenoliths from the Pliocene basantes of the Dzhilinda river were determined: (1) high-T ga- and sp-lherzolites, (2) low-T sp-lherzolites and harzburgites, (3) low-T titaniferous sp-lherzolites. Peridotites of the series 1 have coarse-grained protogranular texture. Peridotites of the series 2 were divided into 2a-coarse-grained protogranular harzburgites and lherzolites (cpx less than 7%), 2b-medium-grained lherzolites, and 2c-fine-grained tabular equigranular lherzolites. Peridotites of the series 2c are often observed in contact with Al-poor pyroxenites. Series 3 titaniferous peridotites enriched in pyroxenes and sp were newly detected. They have a fine-grained mosaic equigranular texture and modal composition: ol=45-50, opx=25-45, cpx=20-22, sp=4-6%.

Minerals of series 1 and 2 have usual peridotite characteristics. Cpx of series 1 have lower Ca# and vary in Mg-number between 87.5 and 91 (Fig.5b). Cpx of series 2 peridotites have higher Ca# and vary in Mg-number between 87 and 94 (Fig.5b). Ol are $Fo_{88.5-91}$ and contain 0.3-0.5 wt.% NiO. Sp is Cr-rich in harzburgites of 2a (Cr#=30-40). In other xenoliths sp have lower Cr#=7-20. Minerals of series 3 peridotites have a specific chemistry. Cpx (Mg number=92-93) contain 2-2.2 wt.% TiO_2. Ol (Fo_{91-92}) contain 0.7 wt.% NiO. Sp (Mg number=77, Cr#=16-17) contain 0.6-0.7 wt.% NiO and 0.9-1.0 wt.% ZnO.

4.2.2. Cr-diopside pyroxenites

Cr-diopside pyroxenites have coarse equant texture and are completely similar to those from the Miocene picrobasalts. They form Ca-poor and Ca-rich (high-T and low-T) sub-series corresponding to the peridotites of series 1 and 2a-b (Fig.5c). The Al-poor pyroxenites are characterized by low contents of Al_2O_3=3-4 wt.% and Na_2O=0.2-0.5 wt.% in cpx. Regarding to mineral composition, these are close to low-temperature peridotites of the series 2c.

4.2.3. Megacryst assemblages

The megacrystic cpx reveal certain trends of compositional variations, such as an increasing in TiO_2, Al_2O_3, CaO, REE and decreasing in Cr_2O_3, while Mg-number decreases (Fig.5c). These features are similar to those for the megacryst assemblage from the Miocene picrobasalts. Abundant ilmenite, ga, Ti-biotite, alkaline feldspar megacrysts were also found in the Pliocene basanites. They have chemistry similar to the megacrysts from the Miocene picrobasalts and have been described in detail by Litasov and Ashchepkov (1996).

4.2.4. Low pressure cumulates

Al-augite pyroxenites contain dark-green cpx and have transitional varieties to lower-T Cr-diopside pyroxenites. They have metacumulative texture and correspond to the subgroup (c) of low-pressure

Table 3. Representative major element composition (wt.%) of xenolith minerals.

Vitim volcanic field, Miocene picrobasalts

Sample	Ga websterite (V-231)				Ga lherzolite with amp-phl-cpx-vein (V-462)							Ilm-bearing ga harzburgite (L-10-2)					
Mineral	cpx	opx	ol	gar	cpx-L	cpx-v	opx	ol	gar	amp	phl	cpx	opx	ol	gar	ilm	phl
Group	3a				2							2					
SiO_2	51.81	54.33	40.88	42.04	51.82	50.99	54.06	40.47	42.28	42.11	37.59	52.10	53.75	39.85	42.01		37.40
TiO_2	0.94	0.24		0.24	0.67	1.51	0.34		0.19	4.28	6.21	0.56	0.56		0.34	53.36	7.26
Al_2O_3	6.67	3.66		22.92	6.12	7.17	3.77		22.50	13.18	15.45	8.35	4.74		22.42	1.34	15.49
Cr_2O_3	0.28	0.12		0.30	1.27	0.16	0.08		1.11	0.59	0.45	0.75	0.50		1.13	3.00	0.95
FeO	3.48	7.38	10.05	8.63	3.99	4.99	7.87	11.15	7.49	7.12	5.93	3.33	6.73	11.61	8.36	27.25	5.42
MnO	0.07	0.11	0.16	0.28	0.10	0.09	0.16	0.12	0.29	0.08	0.00	0.12	0.11	0.11	0.28	0.23	0.02
MgO	14.89	32.21	49.62	20.11	15.05	14.67	31.53	48.24	20.66	14.95	18.86	14.83	30.74	47.36	20.34	13.63	18.33
CaO	18.44	0.79	0.04	4.62	17.75	16.69	0.92	0.06	5.08	9.50	0.41	17.43	0.99	0.06	4.69		0.02
NiO		0.11	0.38					0.34		0.11	0.23			0.37		0.32	0.21
Na_2O	2.20	0.18		0.04	2.24	2.51	0.22		0.02	3.01	0.79	2.45	0.20				0.63
K_2O										1.78	8.96						8.83
Total	98.77	99.13	101.1	99.18	99.01	98.79	98.94	100.4	99.61	96.71	94.87	99.92	98.32	99.36	99.57	99.13	94.56
Mg#	88.4	88.6	89.8	80.6	87.0	84.0	87.7	88.5	83.1	78.9	85.0	88.8	89.1	87.9	81.3		85.8

Sample	Web (V-14)		Ga web (V-211)			Cpx-meg (V-340)			Gar granulite (V-210)				Sp websterite (V-244)				
Mineral	cpx	opx	cpx	opx	gar	cpx	ilm	phl[1]	cpx	opx	gar	sp	cpx	opx	sp	amp	phl
Group	5a		5b			5c			6a				6c				
SiO_2	52.59	54.53	51.27	52.87	41.76	51.50		36.91	47.85	50.38	39.90		49.49	51.77		40.73	36.05
TiO_2	0.33	0.12	0.49	0.27	0.32	0.82	46.54	8.41	0.94	0.14	0.17	0.06	0.96	0.12	0.18	3.69	6.57
Al_2O_3	5.07	4.06	7.21	5.58	22.67	7.21	1.41	15.67	8.69	5.56	21.82	60.11	6.06	3.23	57.57	12.83	14.22
Cr_2O_3	0.77	0.59	0.08	0.09	0.12	0.14	0.02	0.01	0.00	0.00	0.00	0.00	0.17	0.08	9.02	0.21	0.27
FeO	4.80	6.41	7.38	11.26	11.01	3.82	46.86	12.32	8.03	17.62	20.31	26.22	8.27	19.08	16.15	11.94	11.86
MnO	0.10	0.13	0.11	0.16		0.06	0.16	0.03	0.12	0.19	0.76	0.07	0.23	0.33	0.09	0.12	0.04
MgO	19.58	32.35	16.52	28.35	18.03	14.96	5.31	14.10	11.10	25.85	13.14	13.24	11.77	24.65	17.39	12.07	14.12
CaO	15.10	0.95	14.44	1.42	4.93	18.00		0.21	20.44	0.38	4.73		19.73	0.49		10.92	0.03
NiO												0.21	0.01	0.02	0.27		0.03
Na_2O	1.06	0.21	1.70	0.26	0.08	2.34		0.11	1.51	0.06	0.03		2.03	0.06		2.38	0.38
K_2O								6.26								1.74	9.03
Total	99.40	99.34	99.20	100.3	98.93	98.84	100.3	94.51	98.68	100.2	100.9	99.91	98.72	99.83	100.7	96.63	92.61
Mg#	87.9	90.0	80.0	81.8	74.5	87.5		67.1	71.1	72.3	53.6		71.7	69.7	65.7	64.3	68.0

Vitim volcanic field, Pliocene basanites.

Sample	Ga lherzolite (701-11B)				Sp lherzolite (D-871)				Sp lherzolite (D-73)				Sp lherzolite (D-43)			
Mineral	cpx	opx	ol	gar	cpx	opx	ol	sp	cpx	opx	ol	sp	cpx	opx	ol	sp[2]
Group	1a				1a				1b				1c			
SiO_2	51.99	54.45	40.86	42.58	51.64	54.40	41.31		52.90	55.80	40.98		50.45	55.70	41.25	
TiO_2	0.35	0.11		0.19	0.45	0.14		0.21	0.11	0.04		0.09	1.91	0.20		0.22
Al_2O_3	6.83	5.29		22.42	6.56	5.06		56.95	4.47	3.35		48.82	6.94	3.20		52.70
Cr_2O_3	1.15	0.59		1.46	0.76	0.43		11.04	1.17	0.46		20.49	1.14	0.37		15.23
FeO	3.39	5.91	9.53	6.63	3.11	6.47	9.84	11.07	2.44	5.82	9.27	11.84	2.05	5.63	8.42	10.85
MnO	0.13	0.12	0.13	0.30	0.08	0.15	0.12	0.09	0.07	0.15	0.08	0.13	0.05	0.09	0.09	0.11
MgO	16.33	31.66	49.39	21.17	15.75	31.60	49.31	20.25	15.35	33.10	49.65	18.51	13.79	34.00	50.36	19.36
CaO	17.33	1.19	0.14	4.85	19.35	0.97	0.09		21.27	0.63	0.03		21.02	0.37	0.04	
NiO			0.33				0.35	0.40			0.38	0.36			0.73	0.62
Na_2O	1.64	0.21			1.83	0.19			1.28	0.08			2.00	0.05		
Total	99.14	99.53	100.4	99.60	99.54	99.41	101.0	100.0	99.06	99.43	100.4	100.2	99.35	99.61	100.9	100.5
Mg#	89.6	90.5	90.2	85.1	90.0	89.7	89.9	76.5	91.8	91.0	90.5	73.6	92.3	91.5	91.4	76.1

Udokan volcanic field, Pliocene basanites

Sample	Sp harzburgite (74-8)				Sp dunite (74-Du)				Sp lherzolite (74-5)				Lher/web (74-117)			
Mineral	cpx	opx	ol	sp	cpx	opx	ol	sp	cpx	opx	ol	sp	cpx	opx	ol	sp
SiO_2	52.91	55.79	40.59		52.76	55.59	40.66		51.19	54.62	40.60		51.03	53.79	40.50	
TiO_2	0.09	0.04		0.11	0.12	0.04		0.09	0.50	0.12		0.18	0.61	0.15		0.11
Al_2O_3	3.84	2.70		35.58	4.06	2.61		34.88	6.17	4.10		55.75	8.53	5.70		63.41
Cr_2O_3	1.01	0.58		33.39	1.15	0.52		33.70	0.75	0.32		12.55	0.47	0.19		4.58
FeO	2.66	5.64	9.01	13.69	2.77	5.69	9.05	13.67	2.95	6.35	10.15	11.80	2.51	6.08	10.41	9.90
MnO	0.08	0.12		0.16	0.10	0.13		0.17	0.08	0.14		0.10	0.09	0.12		0.07
MgO	16.83	33.53	49.59	16.83	16.76	33.79	49.79	16.77	15.52	32.98	48.73	20.00	14.01	32.68	48.75	21.29
CaO	19.58	0.80	0.07		19.48	0.75	0.05		19.37	0.58	0.06		19.48	0.46	0.05	
NiO			0.36	0.24			0.37	0.24			0.39	0.35			0.40	0.45
Na_2O	1.68	0.14			1.77	0.13			1.84	0.12			2.20	0.09		
Total	98.68	99.34	99.62	99.99	98.97	99.26	99.92	99.53	98.38	99.33	99.93	100.7	98.93	99.25	100.1	99.80
Mg#	91.9	91.4	90.7	68.7	91.5	91.4	90.7	68.6	90.4	90.2	89.5	75.1	90.9	90.5	89.3	79.3

Abbreviations: cpx - clinopyroxene, opx - orthopyroxene, ol - olivine, ga - garnet, sp - spinel, amp - amphibole, phl - phlogopite, ilm - ilmenite. Rock types: web - websterite, lher -lherzolite, Superscripts: 1- F=0.46 wt.%, 2- V_2O_5=0.38 wt.% and ZnO=0.98 wt.%.

cumulate xenoliths from the Miocene picrobasalts (Fig.5a and c). Hydrous minerals were not detected.

4.3. Xenoliths from Pliocene basanites, Udokan field

Cr-diopside group xenoliths of Kuas Lake may be divided into (a) sp-lherzolites, (b) sp-harzburgites and dunites, and (3) sp-websterites and related pyroxene-rich lherzolites. Lherzolites have protogranular to porphyroclastic texture. Harzburgites have coarse-grained protogranular texture with ol grain size up to 1.5 cm, and sometimes contain dunite veins where ol grains reach 3 cm in size. Websterites often contain unusual coarse sp (grain size up to 2 cm) and have been found in contact with lherzolites.

Cpx in lherzolites have transitional composition between those from harzburgites and websterites (Fig. 5d). Mg-number varies between 89 and 94. Opx in most xenoliths have Mg-number from 89.5 to 93 and contain 2.2-5.7 wt.% Al_2O_3. Composition of ol in most nodules is $Fo_{89.3-91.5}$. Mg-number increases from websterites to dunites. NiO contents of ol vary within 0.31-0.41 wt.%. Sp vary in Cr# from 42 in dunites and harzburgites to 3-5 in websterites.

5. Trace element chemistry

Selected trace element analyses of cpx from xenoliths are presented in Table 4. Sp- and ga-peridotites from the Vitim volcanic field are relatively fertile in major element composition (Ionov et al., 1993), and available trace element analyses show that they have quite uniform rare-earth element (REE) patterns and thus form a REE-homogenous peridotite substrate. Strongly depleted peridotite compositions are scarce.

Table 4. Representative trace element data for xenolith minerals.

	V-231			V-462					V-210			V-244		D-871	D-73	D-43	74-Du	74-5	74-117
	cpx	opx	gar	cpx-v	cpx-L	opx	gar	amp	cpx	opx	gar	cpx	amp	cpx	cpx	cpx	cpx	cpx	cpx
Ba	1.44	0.04	0.03	0.23	0.13	0.05	0.03	137	0.25	0.03	0.03	0.59	510	1.31	0.87	0.72	0.97	0.63	0.66
Th	0.05	0.02	0.01	0.15	0.09	0.01		0.07	0.08	0.01	0.01	0.04	0.04	0.17			0.45	2.13	0.35
Nb	0.62	0.04	0.07	1.18	1.09	0.06	0.10	39.7	0.15	0.01	0.03	0.30	22.4	0.61	0.33	0.29	1.76	1.03	0.27
La	2.60	0.01	0.01	3.53	2.80	0.01	0.01	3.23	8.45	0.03	0.01	10.8	16.4	2.50	0.85	0.18	26.0	14.6	3.16
Ce	8.71	0.05	0.09	13.2	9.55	0.05	0.06	10.9	32.9	0.17	0.12	44.4	58.5	4.67	2.19	0.72	67.3	17.2	7.33
Sr	84.4	0.50	0.23	101	106	0.75	0.23	279	32.9	0.24	0.22	151	561	87.6	37.0	39	424	133	87.2
Nd	10.8	0.07	0.63	15.88	10.2	0.12	0.38	11.8	32.0	0.18	1.79	47.6	60.3	4.66	1.32	3.12	37.2	5.31	6.56
Zr	38.4	1.56	27.2	194	43.5	7.33	30.7	118	44.5	2.84	23.7	102	75.3	23.0	2.00	22.8	138	25.3	38.6
Sm	2.93	0.03	0.65	4.55	2.57	0.03	0.48	3.07	6.40	0.05	2.01	12.9	12.6	1.80	0.38	1.46	7.36	1.83	2.50
Eu	0.94	0.01	0.34	1.24	0.78	0.03	0.32	0.82	2.06	0.03	1.26	3.02	3.45	0.64	0.14	0.67	1.99	0.77	0.88
Ti	5330	1213	1385	7729	4027	2130	1104	25425	5211	980	781	5653	24472	2639	502	11129	679	2804	3070
Dy	2.02	0.07	4.28	3.10	1.67	0.10	4.47	2.05	3.27	0.07	8.14	9.53	9.35	2.10	1.12	4.05	3.66	3.84	4.48
Er	0.65	0.04	3.42	1.15	0.59	0.05	3.35	0.56	1.12	0.03	5.23	4.83	4.80	1.21	0.88	2.58	1.50	2.26	3.24
Y	6.17	0.33	33.8	10.2	5.01	0.52	35.2	6.33	10.7	0.21	52.1	38.3	47.14	9.06	7.10	22.1	12.7	18.4	24.54
Yb	0.67	0.03	4.27	0.97	0.59	0.06	3.60	0.58	1.02	0.03	5.62	4.92	5.14	0.86	0.98	2.73	1.37	2.24	3.19

The differences in trace element chemistry of cpx between the pyroxenite groups from the Miocene picrobasalts are characterized by the REE and high field strength elements (HFSE; Nb, Zr, and Ti). For the REE, most clinopyroxenes show a convex-upward pattern on mantle-normalized abundance plots, whereby

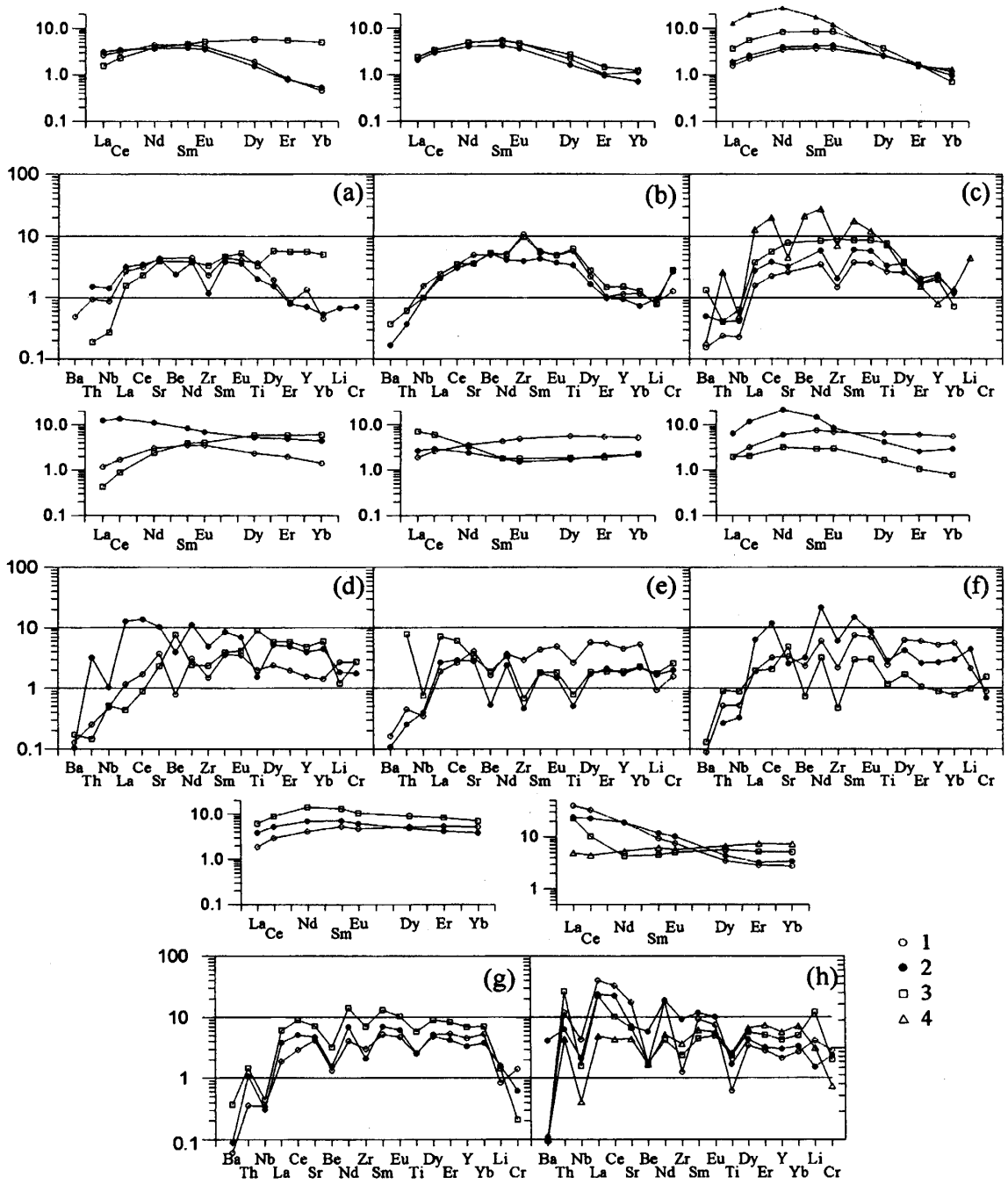

Fig. 6. Primitive mantle normalized (after McDonough, Sun, 1995) trace element patterns of clinopyroxenes from the Vitim (a-g) and Udokan (h) xenoliths. Miocene picrobasalts: (a) 1 - ga lherzolite, 2 - ga-websterite, 3 - sp-lherzolite; (b) 1 - Amp-phl-cpx-vein in lherzolite, 2 - ilm-phl orthopyroxenite, 3 - phl-rich harzburgite; (c) megacryst assemblage: 1 - Cr-rich websterite, 2 - ga-websterite, 3 - cpx megacryst, and 4 - ga-bearing gabbro (lower crustal group). Pliocene basanites: (d) 1-2 - lherzolite, gr.1, 3 - Ti-rich lherzolite, gr.3; (e) lherzolites, gr.2a and 2b; (f) 1 - lherzolite, gr.2c, 2 - Al-poor websterite, 3 - Al-poor graphite-bearing websterite from picrobasalt; (g) 1 - Cr-diopside sp-websterite, 2-3 - Al-augite sp-websterite. Kuas Lake basanites (h): 1 - dunite, 2 - harzburgite, 3 - lherzolite, 4 - websterite.

light REE (LREE) have higher normalized abundances than heavy REE (HREE), and the peak position is at or close to Nd (Fig.6). Th usually approximates an extrapolation of the REE pattern, whereas the HFSE, Ba and Be vary widely. Be exhibits behavior similar to that of the HFSE, and large variations in Be/Nd, Zr/Sm, Ti/Eu ratios are between different pyroxenite groups. Fig.6a-c shows a summary of cpx patterns from the pyroxenite groups. The patterns for the cpx from Cr-diopside pyroxenites and megacrysts are generally similar, whereas all the group 3 samples are definitely different.

Vein cpx is slightly enriched in REE and depleted in Cr, and the cpx patterns have Zr- and Ti-peaks (Fig.6b). A negative anomaly for Zr and Ti in cpx is normal for ultramafic systems (Rampone et al., 1991), whereas a positive anomaly is unusual. In the rare cpx from ilmenite-bearing orthopyroxenites, however, there is no Zr- and Ti-anomaly, presumably due to an uptake of HFSE in ilmenite.

Trace element patterns for the cpx from megacrystic pyroxenites are shown in Fig.6c. The Cr-rich varieties are LREE-depleted and HREE-enriched with negative Zr- and Ti-anomalies, whereas the Cr-poor group with lower Mg-number is richer in LREE, HFSE, Ba, and Th without relative enrichment in HREE. Trace element patterns for the cpx from series 1 and 2 peridotite of the Pliocene basanites are indicative for a low degree partial melting of the primitive mantle. However, 2a-harzburgites contain LREE-rich, HFSE-poor cpx: (La/Yb)n=1.2-3.5 and (Ti/Eu)n=0.2-0.4 (Fig.6d-e). Peridotites of series 2c contain cpx with slightly convex-upward REE patterns and low HFSE, Sr contents. The same patterns are characteristic for the Al-poor Cr-diopside pyroxenite (Fig.6f). REE patterns for the cpx from series 3 peridotites are very unusual. They have low (La/Yb)n=0.01-0.08 suggesting an evidence for MORB-like composition of coexisting melt (see below) and positive Nb, Be, Ti, and light negative Zr anomaly (Fig.6d). Cpx REE patterns of Cr-diopside pyroxenites and Al-augite low pressure cumulates are quite similar with (La/Yb)n=0.3-5.1 (Fig.6g).

The most cpx from the Udokan peridotites is enriched in LREE and variably depleted in HFSE (Fig.6h). The cpx from lherzolite and websterite is distinguished from those from harzburgite. Cpx from websterite have flat REE distribution, significant negative Nb- and light Zr- and Ti-anomaly. Cpx from lherzolite has U-shape patterns with LREE-enrichment. Harzburgite contains cpx with strong LREE and less MREE-enrichment and HFSE-depletion. The most LREE-enriched cpx was found in harzburgite containing dunite veins.

6. P-T estimations and mantle section modelling

Pressure-temperature estimations based on the mineral equilibrium for the Vitim xenoliths were reported for the lherzolites by Ionov et al. (1993) and Litasov (1996) and for the pyroxenites by Ashchepkov et al. (1994). Results for the current sample set are shown in Fig.7 using T-estimations after

Brey and Kohler (1990) and P-estimations after Nickel and Green (1985). The Wells (1977) thermometer was used to estimate equilibration temperatures for the Fe-rich lower crustal assemblages, because the most of available thermobarometers for ultramafic assemblages are calibrated for Mg-rich compositions (Brey and Kohler, 1990).

Cr-diopside ga-pyroxenites form a P-T-field linking ga-lherzolite field and megacrystic ga-websterites at P=20-27 kbar and T=1030-1160℃ (Fig.7). P-T-estimations for metasomatic assemblages are restricted to peridotitic parts of infiltrated rocks, as no thermobarometers for the vein assemblages are available. Litasov (1996) showed that P-T-estimations for the peridotitic assemblages were compatible with equilibration of amp-bearing rocks at shallower depth (23-18 kbar) and slightly lower temperatures than phl-bearing ones (28-20 kbar). These estimations are consistent with the amp and phl stability fields in the upper mantle peridotites (Wallace and Green, 1991; Mengel and Green, 1989).

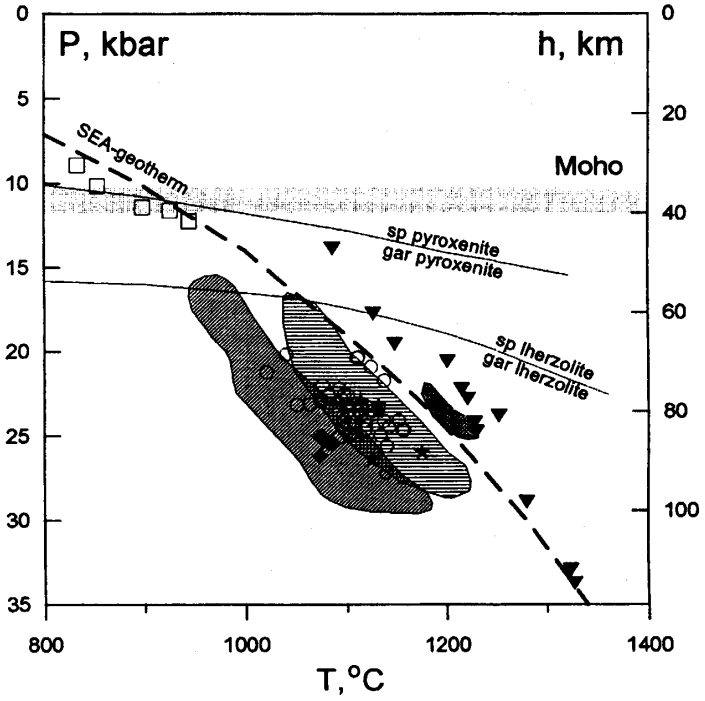

Fig. 7. P-T-fields for the Vitim xenoliths based on the combination of the Brey & Kohler (1990) thermometer and Nickel & Green (1985) barometer. Symbols are as in Fig. 5a. The southeastern Australia geotherm (SEA: O'Reilly and Griffin, 1985) is shown for a comparison. Solid lines are boundaries between fertile sp- and ga-lherzolite with Mg#=0.90 and Cr#Sp=0.10 (O'Neill, 1981) and between ga- and gp-plagioclase pyroxenites in CMAS system (Herzberg, 1978). Fields outline T-P estimations for ga- and ga-sp-lherzolites from picrobasalts after Ionov et al. (1993) and Ashchepkov et al. (1994) - inclined hatching, ga- and ga-sp-lherzolites from the Pliocene basanites of Bulykhta River and Kandidushka Volcano - horizontal hatching, Dzhilinda ga-lherzolites - crossed hatching.

Ga-websterites of megacryst trend form a hotter and well-defined geotherm (Fig.7) with P-estimations ranging from 14 to 30 kbar and temperature from 1060 to 1320℃. Cr-rich megacrystic websterites were formed at 1300-1380℃. Their T-projection on the geotherm (not shown in Fig.7) corresponds to 30-35

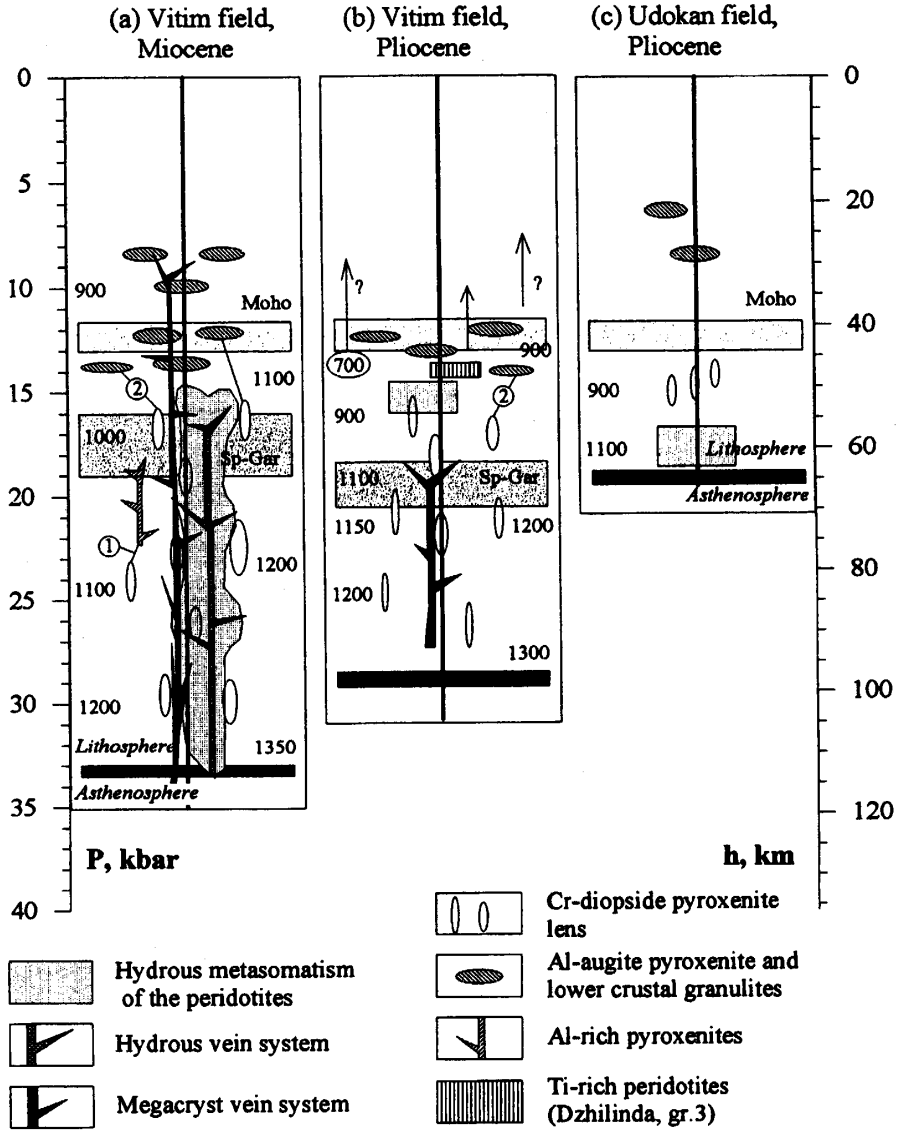

Fig. 8. Mantle sections beneath the Vitim and Udokan field built from xenoliths data. More complex section is drawn beneath the Vitim field due to wide development of enrichment processes - modal metasomatism, fracturing and melt fractionation in the mantle - megacryst and pyroxenite assemblages. Note presumed genetic correlations between (1) Cr-diopside and Al-rich pyroxenites, and (2) Cr-diopside and Al-augite pyroxenites. Temperature estimations for peridotite (right side) and pyroxenite (left side) are also shown. Present time position of Moho boundary is shown after geophysical data by Zorin et al. (1989). This data poorly corellate with petrologic evidence for the Dzhilinda peridotites. Some of them correspond to the depths of 30-40 km due to low T-estimations. If these xenoliths have been derived from the greater depths, it denotes a very gentle slope of the geotherm. Lithosphere-asthenosphere boundary after Litasov (1996).

kbar.

P-T estimations using Wells (1977) thermometer and Nickel and Green (1985) barometer for low-pressure ga-granulites correspond to the lowermost crust and uppermost mantle: P=7-12 kbar, T=820-960℃ (Fig.7). The similar T-estimation for subgroup (c) sp websterites suggests a similar position close to the mantle-crust boundary.

P-T-estimations for the series 1 peridotites from the Pliocene basanites correspond to the depths 60-80 km at T=1100-1250℃. Lower temperature peridotites of series 2 and 3 correspond to the depths 40-50 km at T=800-900℃ and 750-850℃ respectively. Cr-diopside pyroxenites, as well as peridotites, form high- T (1050-1230℃) and low-T (860-1000℃) sub-series. Field of P-T estimations for peridotites from the Pliocene basanites 50-100℃ hotter than that for peridotites from the Miocene picrobasalts. Moreover, ga-bearing nodules from Dzhilinda River reveal the highest estimated temperatures (Fig.7).

Among the Kuas Lake peridotites, harzburgites and dunites seem to indicate higher temperatures than lherzolites and websterites. T-estimations for harzburgite range within 980-1120℃, for lherzolite within T=900-1090℃, and for websterite within T=900-1050℃. Mantle columns reconstructed from termobarometry data are shown in Fig. 8.

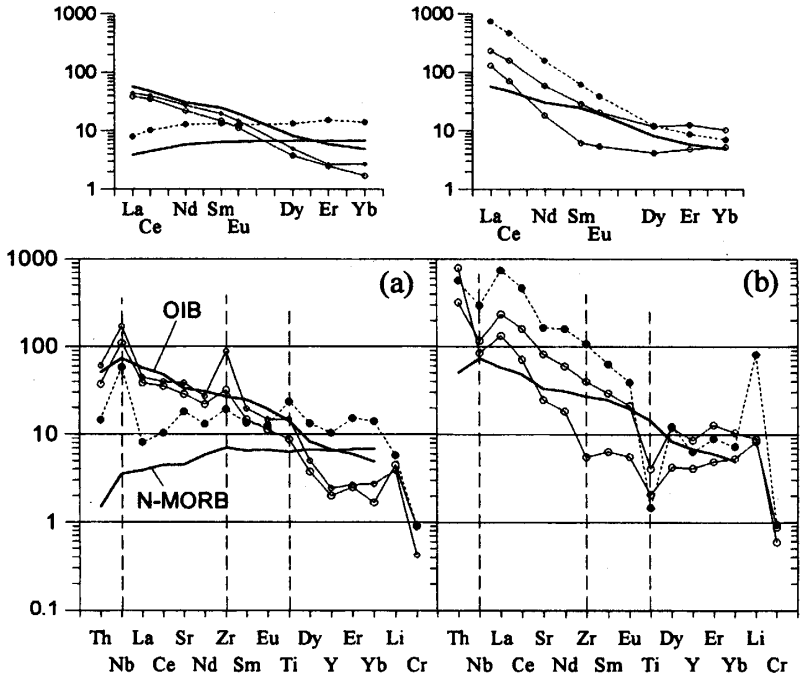

Fig. 9. Composition of melt coexisting with clinopyroxene from pyroxenite and perdotite xenoliths, normalized to primitive mantle after McDonough and Sun (1995). (a) HFSE-rich patterns: open circles - metasomites from picrobasalts, filled circles - Ti-rich peridotites, gr.3 (Dzhilinda River); (b) HFSE-poor patterns: open circles - Dzhilinda peridotites, gr.2a and 2b, filled circles - dunite, Kuas Lake (Udokan field). OIB and N-MORB (after Sun and McDonough, 1989) are shown by thicker lines. Partition coefficients were used after Hart and Dunn (1993).

7. Discussion

Present results and other geochemical data available for the Vitim and Udokan xenoliths indicate that the influence of four major melt types is recorded in mantle-derived xenoliths.

(1) Cr-rich melt migrating along small fractures and continuously reacting and reequilibrating with wall peridotite, forms rocks with Cr-diopside pyroxenites and LREE-rich harzburgites as endmembers (Fig.9b). This type of melt undergoes the process of percolative fractionation.

(2) MORB-like Ti-rich melt forms the series 3 titaniferous peridotite (Dzhilinda) (Fig.9a).

(3) Picrobasaltic to alkaline-basaltic melt producing the volcanics of the Vitim field is represented also by the group a-b megacrystic pyroxenites. These pyroxenites suffered fractionation in large hydraulic fractures or magma chambers.

(4) HFSE and volatile-enriched melts produced amp- and phl-bearing vein assemblages and related pyroxenite types (Fig.9a).

7.1. Xenoliths from the Miocene picrobasalts, Vitim field

The Cr-diopside-rich pyroxenites are probably products of mantle anatexis and small-scale percolation of resultant melts. This process has been termed "percolation fractionation" (Harte et al., 1993) or "paratexis" (Dobretsov, 1981). REE patterns in the Vitim chromdiopside vary from LREE-depleted to strongly enriched ones relative to OIB (LREE contents in coexisting melt are 1-3 times and Ba, Th contents 4-7 times higher than in OIB). It may indicate crystallization from melts undergone various degrees of differentiation, although observed enrichment in trace elements, which are more incompatible than Ce, may also result from reaction during percolation (Vernieres et al., 1997). However, percolative fractionation and reequilibration with peridotite matrix alone cannot account for all variations in Cr, REE-contents and texture features of the Vitim xenoliths. Transitional textures from peridotite towards the cumulates may be explained by segregation of melt evolved by percolative fractionation to larger fractures, where pyroxenites with cumulate texture have been formed. Cr-depletion and Al-enrichment of coarse-grained websterites are characteristic for the transition from percolative to fracture fractionation process.

The calculated melt compositions in equilibrium with megacryst assemblages are similar to the host volcanics. The mechanism of megacryst formation as a pulsatory polybaric fractionation of basaltic melt was described by Ashchepkov et al. (1995). The megacryst compositions form two major clusters which may be ascribed to subgroups a and b in Fig. 5. A-subgroup Cr-rich websterites were formed at the greatest depths and highest temperatures (3.0-35 kbar, T=1300-1380℃). Their origin may be explained by buffering of the melt composition by the peridotite wall rocks (e.g. Eggler, 1979). Group b ga-websterite and clinopyroxenite with numerous sulfide inclusions were formed at the depths about 15-30 kbar,

resulting from progressive crystallization through the sequence Cpx+Ga+Opx, Cpx+Ga, and Cpx alone. Finally, titaniferous Cpx megacrysts with spongy rims containing abundant fluid inclusions, occasional ilmenite and phl inclusions were formed at pressures of approximately 15-11 kbar and T=900-1000℃.

Major metasomatic agent beneath the Vitim volcanic field is a HFSE- and volatile-rich melt. The process resembles Fe-Ti-K-rich metasomatism often described in xenoliths from continental basalts (Menzies et al., 1987b; Kempton, 1987). However, it has a specific HFSE-enrichment, which is characteristic also for the other volcanic fields of the Baikal Rift region (Ionov and Hofmann, 1995; Ionov et al., 1997). From the mineral chemistry, we suggest that the amp- and phl-bearing assemblages have been formed due to an infiltration of small melt fractions. The chemical features of interstitial cpx and amp around veins become distinct from vein minerals and acquire characteristics resembling wall peridotite minerals due to re-equilibration with them. The chilling and crystallization of small melt fractions preserve local trace element patterns with curious HFSE characteristics (Fig.6b). The formation of orthopyroxenite by reaction of crack-filling melt with peridotite conforms to experimental data provided by Sen and Dunn (1995), where an opx-bearing zone has been formed between amphibolite and peridotite. An opx-rich reaction zone replacing original peridotite was also found at higher pressures, where basaltic melt from high-degree melting of eclogite contacted to wall peridotite (Yaxley and Green, 1998).

The mineral chemical characteristics and thermobarometric estimations for the Vitim low-pressure pyroxenites are consistent with formation of intrusive bodies near the crust-mantle boundary and within the lower crust. Similar origin related to underplating was suggested for lower crustal xenoliths from other areas (Downes, 1993; Kempton et al., 1995). Major and trace element composition of group (a) ga-clinopyroxenites is close to that of the most fractionated megacryst assemblages. Similar xenoliths from Shavaryn-Tsaram volcano in Mongolia, which is also related to the Baikal Rift zone, have a Sm-Nd age near zero (Stosch et al., 1995) showing a relation between lower crustal pyroxenite formation and modern volcanic activity. Group c sp-websterites are apparently related to Cr-diopside pyroxenites, which is evident from the occurrence of transitional nodules between these two types and from REE patterns of cpx. Group b ga-granulites could be derived from both melt types, but the chemical compositions of amp, phl, and cpx suggest their closer relation to Cr-rich melt derivates.

7.2. Xenoliths from the Pliocene basanites, Vitim field

Protogranular peridotites of the series 1 represent primitive or slightly depleted mantle from the depths 60-80 km at T=1100-1250℃. Trace element patterns in cpx are indicative for low degree partial melting of the primitive mantle. Most of the series 2 peridotites contain the same primitive or slightly LREE-depleted cpx and correspond to the depths 40-50 km at T=800-900℃. LREE-enriched patterns of some cpx from

peridotites of the Dzhilinda Pliocene basanites are partly resembling with those found among Udokan nodules (Fig. 9) and were probably formed by percolating melt-peridotite reaction (see below).

Titaniferous peridotites of series 3 were newly detected. T-estimations within 750-850℃ suggest their correspondence to the uppermost mantle section (40-50 km depth). Melt coexisting with cpx has REE pattern similar to N-MORB, although it has, in addition, significant Nb, Zr, Ti positive peaks. Numerical modeling of partial melting and melt percolation shows that the most suitable agent is a basaltic melt derived from ilmenite-phl-bearing sp-lherzolite (probably vein assemblage). Ilmenite in the source is responsible for high contents of V, Ni, Zn, Ti. Very high contents of compatible elements in peridotite of group 3 and magnesian composition of minerals suggest for significant primary depletion - more than 15% of primitive mantle melting. Trace element variations allow to assume as a primary assemblage the dunite or harzburgite with high Sp-contents (>3%). Thus, unique Ti-rich peridotite of Dzhilinda River characterizes rare type of shallow mantle-melt interaction newly detected among the Vitim xenoliths.

REE distribution in cpx from sp-websterites (Fig.6g) is explained by fractional crystallization of melt coexisting with Cr-diopside pyroxenites (Litasov, 1999) as well as for the sp-websterites from Miocene picrobasalts. Cpx megacrysts were formed by fractional crystallization of alkaline basaltic or picrobasaltic melts similar to those reported for the megacryst assemblage from the Miocene picrobasalts (see above).

7.3. Xenoliths from the Pliocene basanites, Udokan field

The variations in modal and major element composition in the Kuas peridotites most likely result from different degrees of partial melting and melt extraction from the fertile mantle source which is strongly suggested by the whole rock correlation of MgO with Al, Ca etc. However study of trace element chemistry of cpx indicates an absence of typical LREE-depleted trace element patterns characterizing simple partial melting.

Cpx from depleted Kuas peridotites shows a range of trace element enrichment due to an interaction with mantle fluids or small melt fractions. Different authors consider the interaction of peridotite with carbonatitic or basaltic melts/fluids showing significance of both processes in the lithospheric mantle (Hauri et al., 1993; Bedini et al., 1997; Ionov, 1998). Changes of cpx REE-composition are in agreement with the percolation-reaction model by Vernieres et al. (1997) considering reactive porous flow at the transition between convecting and lithospheric mantle. Harzburgite corresponds to the lower (high-T) part of the mantle section column and contains cpx with most evolved REE patterns reflecting melting reaction. Lherzolite corresponds to the middle part of domain, and websterite with least evolved cpx composition belongs to the upper part of column and is formed by the pyroxene-forming reaction with decreasing melt fraction. REE patterns of melts coexisting with all the cpx are unrelated to the host magmas. This model is

different from example presented by Bedini et al. (1997) for Ethiopian xenoliths, where most LREE-enriched patterns correspond to the upper part of mantle section. Here we suggest that LREE-enriched patterns of harzburgitic cpx correspond to the continous reaction with melt at the base of lithosphere.

8. Conclusions

1. The comparison of three xenolith sets from the Vitim (Miocene and Pliocene) and Udokan (Pliocene) volcanic fields of the eastern part of Baikal Rift System revealed that the upper mantle section beneath the Vitim is more complex than beneath the Udokan due to wide development of enrichment processes - modal metasomatism, fracturing and melt fractionation (megacryst and pyroxenite assemblages).

2. Peridotite xenoliths from the Vitim Miocene picrobasalt represent garnet and spinel depth facies. Pyroxenite xenoliths are the products of three melt types. The first, forming Cr-diopside pyroxenites, is an interstitial melt migrating through peridotite matrix. It is similar to melts described in peridotite massifs as undergone percolative fractionation. The second and third melt types form the hydrous veins and megacrystic pyroxenites, respectively. Both crystallize in channels, whereby the amphibole- and phlogopite-bearing assemblages represent smaller channels of dozen centimeter scale.

3. Peridotite xenoliths from the Vitim Pliocene basanites are divided into series: (1) high-T garnet and spinel lherzolites; (2) low-T spinel lherzolites and harzburgites; (3) low-T titaniferous spinel lherzolites. Series 1 protogranular peridotites represent primitive to moderately depleted mantle of 60-80 km depth at T=1100-1250℃. Clinopyroxene trace element patterns indicate a low degree partial melting of primitive mantle. Series 2 peridotites correspond to 40-50 km depth at T=800-900℃. Series 3 titaniferous peridotites enriched in pyroxenes and spinels are first described having a mosaic equigranular texture and representing rare type of melt/mantle interaction. Estimated 750-850℃ temperatures are projected to the geotherm at the field of uppermost mantle (40-50 km depth). High Ti content (TiO_2=0.55% in the whole rock) may be an evidence for metasomatizing melt generated from ilmenite- and/or phlogopite-bearing source.

4. Xenoliths from the Udokan Pliocene basanites show variations of unhydrous depletion/enrichment process in the lower lithosphere. Xenoliths correspond to spinel peridotite depth facies and are divided into series: (1) lherzolite; (2) harzburgite and dunite; (3) websterite. Depleted nodules contain LREE-enriched and HFSE-depleted clinopyroxene. The enrichment is due to reactive percolation of small melt fraction and accompanying melting of peridotite matrix. Harzburgite-to-dunite veins correspond to the lower part of mantle column and are formed by olivine-producing reaction with melt fraction increasing. Lherzolite and websterite represent the middle and upper part of column and are formed by pyroxene-producing reaction with melt fraction decreasing.

Acknowledgements

The authors are thankful to T. Hasenaka for the comments and revision of the manuscript. K.L. and Y.L. are obliged to the Russian Foundation for Basic Research supporting the grant N97-05-65309. K.L. acknowledges a Center for Northeast Asian Studies (CNEAS), Tohoku University Research Fellowship.

References

Ashchepkov, I.V., Andre, L., Litasov, K.D. and Mal' kovets, V.G.,1995

Origin and evolution of mantle melt beneath Vitim plateau, *Ext. Abst. 6th Int. Kimb. Conf.*, 17-19, Novosibirsk, Russia.

————, Litasov, Yu.D. and Dobretsov, N.L., 1994

Pyroxenites and composite garnet peridotite xenoliths from picrite-basalt, Vitim plateau (Transbaikal): Implication for thermobarometry and mantle reconstruction, *Proc. 5th Int. Kimb. Conf.*, v.1/A, 455-466, Rio-de-Janeiro, Brazil.

Bedini, R.M., Bodinier, J.L., Dautria, J.M., and Morten, L., 1997

Evolution of LILE-enriched small melt fractions in the lithospheric mantle: a case study from the *East African rift, Earth Planet. Sci. Lett.*, 153, 67-83.

Brey, G.P. and Kohler, T., 1990

Geothermobarometry in four-phase lherzolites II. New thermobarometers, and practical assessment of existing thermobarometers, *J. Petrol.*, 31, 1313-1336.

Dobretsov, N.L., 1981

Global petrological processes, Nauka, Novosibirsk (in Russian).

Downes, H., 1993

The nature of the lower continental crust of Europe: petrological and geochemical evidence from xenoliths, *Phys. Earth Planet. Int.*, 79, 195-218.

Eggler, D.H., McCallum, M.E. and Smith, C.B., 1979

Megacryst assemblages in kimberlite from Northern Colorado and Southern Wyoming: petrology, geothermometry-barometry, and areal distribution, *Proc. 2nd Int. Kimb. Conf.*, 213-226.

Esin, S.V., Ashchepkov, I.V. and Ponomarchuk, V.A., 1995

Petrogenesis of alkaline basaltoids from the Vitim plateau (Baikal rift zone), UIGGM SB RAS Press, Novosibirsk.

Frey, F.A. and Printz, M., 1978

Ultramafic inclusions from San Carlos, Arizona: petrologic and geochemical data bearing on their petrogenesis, *Earth Planet. Sci. Lett.*, 38, 129-176.

Glaser, S.M., Foley, S.F. and Gunter, D., 1999

Trace element enrichment by melt infiltration in garnet- and spinel peridotite xenoliths from the Vitim volcanic field, Transbaikalia, eastern Siberia, *Lithos*, 48, 263-285.

Gusev, G.S. and Khain, V.Ye., 1996

On relation between the Baikal-Vitim, Aldan-Stanovoy, and Mongol-Okhotsk terranes (south of mid-Siberia), *Geotectonics*, 29, 422-436.

Hart, S.R. and Dunn T., 1993

Experimental clinopyroxene/melt partitioning of 24 trace elements, *Contr. Mineral. Petrol.*, 113, 1-8.

Harte, B., Hunter, R.H. and Kinny, P.D., 1993

Melt geometry, movement and crystallization, in relation to mantle dykes, veins and metasomatism. In K.G. Cox, D. McKenzie and R.S. White (ed.), *Melting and melt movement in the Earth*, 1-21, Oxford Sci. Publ.

Hauri, E.H, Shimizu, N., Dieu, J.J. and Hart, S.R., 1993

Evidence for hotspot-related carbonatite metasomatism in the oceanic upper mantle, *Nature, 365, 221-227.*

Herzberg, C.T., 1978

Pyroxene geothermometry and geobarometry: experimental and thermodynamic evaluation of some subsolidus phase relations involving pyroxenes in the system CaO-MgO-Al_2O_3-SiO_2, *Geochim. Cosmochim. Acta*, 42, 945-957.

Ionov, D.A. 1998

Trace element composition of mantle-derived carbonates and coexisting phases in peridotite xenoliths from Alkali basalts, *J. Petrol.*, 39, 1931-1941.

———— and Hofmann, A.W., 1995

Nb-Ta-rich mantle amphiboles and micas: Implications for subduction-related metasomatic trace element fractionations, *Earth Planet. Sci. Lett.*, 131, 341-356.

————, Ashchepkov, I.V., Stosch, H.-G., Witt-Eickschen, G. and Seck, H.A., 1993

Garnet peridotite xenolith from the Vitim volcanic field, Baikal region: the nature of the garnet-spinel peridotite transition zone in the continental mantle, *J. Petrol.*, 34, 1141-1175.

————, Griffin, W.L. and O' Reilly, S.Y., 1997

Volatile-bearing minerals and lithosphere trace elements in the upper mantle, *Chem. Geol.*, 141, 153-184.

Kempton, P.D., 1987

Mineralogic and geochemical evidence for different styles of metasomatism in spinel lherzolite

xenoliths: enriched mantle source region of basalts? In M.A. Menzies (ed.), *Mantle Metasomatism*, 45-89, Academic Press, London.

――――, Downes, H., Sharkov, E.V., Vetrin, V.R., Ionov, D.A., Carswell, D.A. and Beard, A., 1995

Petrology and geochemistry of xenoliths from the Northern Baltic shield: evidence for partial melting and metasomatism in the lower crust beneath an Archaean terrane, *Lithos*, 36, 157-184.

Litasov, K.D., 1999

Petrology and Geochemistry of lower crustal xenoliths from alkaline basalts, Vitim plateau, *Geologiya i Geophizika*, 40, 670-689 (in Russian). English edition: *Russ. Geol. Geophys.* (in press).

―――― and Ashchepkov, I.V., 1996

Ilmenite megacrysts and ilmenite-bearing pyroxenites from alkaline basalts, Vitim Plateau, *Russ. Geol. Geophys.*, 37, 7, 97-108.

――――, Rasskazov, S.V., Ivanov, A.V., 1999

Depleted and enriched spinel peridtitite from Cenozoic basanites of the Kuas lake. Udokan range, East Siberia, *Transact. (Doklady) Russ. Acad. Sci.* 367 (6), 803-807.

Litasov, Yu.D., 1996

Petrology of the mantle-derived xenoliths in alkaline basalts from the Vitim plateau, Trans-Baikal: an approach to model for primitive mantle and metasomatic modification, *Ph.D. Thesis*, Hokkaido Univ.

McDonough, W.F. and Sun, S.S., 1995

The composition of the Earth, *Chem. Geol.*, 120, 223-253.

Mengel, K. and Green, D.H., 1989

Stability of amphibole and phlogopite in metasomatized peridotite under water-saturated and water-undersaturated conditions. *Proc. 4th Int. Kimb. Conf.*, 571-581, Geol. Soc. Austr. Spec. Publ., 14.

Menzies, M.A., Arculus, R.J., Best, M.G., Bergman, S.C., Ehrenberg, S.N., Irving, A.J., Roden, M.F. and Schulze, D.J., 1987a

A record of subduction processes and within plate volcanism in lithospheric xenoliths of the southwestern USA, *In* P.Nixon (ed.), *Mantle Xenoliths*, 59-74, Wiley, NY.

――――, Rogers, N., Tindle, A. and Hawkesworth, C.J., 1987b

Metasomatic and enrichment processes in lithospheric peridotites, an effect of asthenosphere-lithosphere interaction, *In* M.A. Menzies (ed.), *Mantle Metasomatism*, 145-220, Academic Press, London.

Mercier, J.C.C., Nicolas, A., 1975

Textures and fabrics of upper mantle peridotites as illustrated by xenoliths from basalts. *J. Petrol.*, 16, 454-487.

Nickel, K.G. and Green, D.H., 1985

Empirical geothermobarometry for garnet peridotites and implications for the nature of the lithosphere, kimberlites and diamonds, *Earth Planet. Sci. Lett.*, 73, 158-170.

O' Neill, H.St.C., 1981

The transition between spinel lherzolite and garnet lherzolite, and its use as geobarometer, *Contr. Mineral. Petrol.*, 77, 185-194.

O' Reilly, S.Y. and Griffin, W.L., 1985

A xenolith-derived geotherm for Southeastern Australia and its geophysical implications, *Tectonophysics*, 111, 41-63.

Rampone, E., Bottazzi, P. and Ottolini L., 1991

Complementary Ti and Zr anomalies in orthopyroxene and clinopyroxene from mantle peridotites, *Nature*, 354, 518-520.

Rasskazov, S.V., 1986

Basaltoids of Udocan (in Russian). Nauka, Novosibirsk.

－－－－, Ivanov, A.V., Brandt, I.S., and Brandt S.B., 1998

Migration of Late Cenozoic volcanism in Baikal and Olekma-Stanovoi systems, *Transact. (Doklady) Russ. Acad. Sci.*, 360, 378-382.

－－－－, －－－－, Boven, A., Andre, L., 1997

Late Cenozoic reactivation of the Early Pre-Cambrian Aldan Shield: trace element constraints on magmatic sources beneath the Udokan Ridge, Siberia, Russia, *In* Lee et al. (eds.), *Proc. 30th Int. Geol. Congr.*, Pt.15, 153-167, Beijing, China.

－－－－,－－－－ and Brandt, S.B., 1996

Development of volcanism with rifting relaxation, detail study of Late Cenozoic Bereya area, Vitim volcanic field, *Proc. Geol. Symp. IEC SB RAS*, 56-58, Irkutsk, Russia (in Russian).

Sen, C. and Dunn, T., 1995

Experimental modal metasomatism of a spinel lherzolite and the production of amphibole-bearing peridotite, *Contr. Mineral. Petrol.*, 119, 422-432.

Sengor, A.M.C., Natal' in, B.A. and Burtman, V.S., 1994

Tectonic evolution of Altaids, *Russ. Geol. Geophys.*, 35, 7-8, 33-47.

Stosch, H.-G., Ionov, D.A., Puchtel, I.S., Galer, S.J.G. and Sharpouri, A., 1995

Lower crustal xenoliths from Mongolia and their bearing on the nature deep crust beneath central Asia, *Lithos*, 36, 227-242.

Sun, S.-S. and McDonough, W.F., 1989

Chemical and isotopic systematic of oceanic basalts: implications for mantle composition and processes, *In* A.D. Saunders, M.J. Norry (eds.), *Magmatism in the ocean basins*, 313-345, Geol. Soc. Spec. Publ., 42.

Takahashi, E., 1986

Origin of basaltic magmas: implications from peridotite melting experiments and an olivine fractionation model, *Bull. Volc. Soc. Japan*, 2, 30, 17-40.

Vernieres, J., Godard, M. and Bodinier, J.-L., 1997

A plate model for the simulation of trace element fractionation during partial melting and magmas transport in the Earth' s upper mantle, *Jour. Geophys. Res.*, 102, 24771-24784.

Wallace, M.E. and Green, D.H., 1991

The effect of bulk rock composition on the stability of amphibole in the upper mantle: implications for solidus positions and mantle metasomatism, *Mineral. Petrol.*, 44, 1-19.

Wells, P.R.A., 1977

Pyroxene thermometry in simple and complex systems, *Contr. Miner. Petrol.*, 62, 129-139.

Yaxley, G.M. and Green, D.H., 1998

Reactions between eclogite and peridotite: mantle refertilisation by subduction of oceanic crust, *Schweiz. Min. Petr. Mitt.*,78, 243-255.

Zorin, Yu.A, Kozhevnikov, V.M., Novoselova, M.R. and Turutanov, E.H., 1989

Thickness of the lithosphere beneath the Baikal rift zone and adjacent regions, *Tectonophysics*, 168, 327-337.